doi:10.1038/nature03639 nature

ARTICLES

Evidence for magmatic evolution and diversity on Mars from infrared observations

P. R. Christensen[1], H. Y. McSween Jr[2], J. L. Bandfield[1], S. W. Ruff[1], A. D. Rogers[1], V. E. Hamilton[3], N. Gorelick[1], M. B. Wyatt[1], B. M. Jakosky[4], H. H. Kieffer[5], M. C. Malin[6] & J. E. Moersch[2]

Compositional mapping of Mars at the 100-metre scale with the Mars Odyssey Thermal Emission Imaging System (THEMIS) has revealed a wide diversity of igneous materials. Volcanic evolution produced compositions from low-silica basalts to high-silica dacite in the Syrtis Major caldera. The existence of dacite demonstrates that highly evolved lavas have been produced, at least locally, by magma evolution through fractional crystallization. Olivine basalts are observed on crater floors and in layers exposed in canyon walls up to 4.5 km beneath the surface. This vertical distribution suggests that olivine-rich lavas were emplaced at various times throughout the formation of the upper crust, with their growing inventory suggesting that such ultramafic (picritic) basalts may be relatively common. Quartz-bearing granitoid rocks have also been discovered, demonstrating that extreme differentiation has occurred. These observations show that the martian crust, while dominated by basalt, contains a diversity of igneous materials whose range in composition from picritic basalts to granitoids rivals that found on the Earth.

High-resolution imaging of the martian surface has allowed the construction of morphologic maps showing considerable diversity at local and regional scales. However, petrology has not kept pace and so virtually no information exists about mineralogic or geochemical variations at comparable spatial scales. Remote sensing data from the Mars Global Surveyor Thermal Emission Spectrometer (TES) and visible/near-infrared (IR) spectroscopy from spacecraft-based and Earth-based telescopes have revealed mineralogic variations between regional-scale units[1–4], but martian igneous and sedimentary processes almost certainly resulted in much more diversity than is presently recognized. Volcanic units are probably composed of materials formed by different degrees of partial melting and modified by fractional crystallization and interaction with crustal compositions during magma ascent and eruption. Similarly, sedimentary units presumably experienced mineral fractionations during transport and deposition, and erosion, tectonic activity and impact may have excavated different subsurface materials at local scales.

THEMIS provides IR spectroscopic data in eight surface-sensing wavelength bands from 6.8 to 13.6 μm at sufficiently high spatial resolution (~100 m per pixel) to identify and map local geologic units having different mineralogies[5]. Here we use a highly effective strategy for compositional mapping that combines THEMIS and TES data, selecting TES pixels within mapped THEMIS units for detailed spectroscopic analysis, to extend the mineralogic mapping achieved with TES[1,2,6–8] to spatial scales relevant to many geologic processes.

Magma evolution in the Nili Patera volcano

Nili Patera forms the northernmost caldera of a caldera complex 400 by 200 km at the summit of the ~1,300-km-diameter Syrtis Major volcanic construct of Hesperian (~2–3 billion years old) age[9] (Fig. 1). Nili Patera is ~50 km in diameter and lies ~1.8 km below the western caldera rim on the basis of MOLA topography[10]. The floor has been domed by ~300 m following the initial emplacement of the floor units, producing a N–S-trending fracture system, with subsequent flows that cross these grabens (Fig. 1a).

Approximately a third of the floor materials (~900 km^2) have unusually high night-time temperatures (208 to 214 K; Fig. 1b) that indicate the presence of bedrock or highly consolidated materials[5]. Barchan dunes, which form through sand transport across a hard surface where sand is limited, are seen on the western portion of these bedrock surfaces (Figs 1 and 2). These dunes formed in a southwest-directed wind regime, suggesting that wind-driven sand may be the erosive agent that has scoured the upwind surface to bedrock. The entire caldera floor, including the dunes, has night-time temperatures $>192 \pm 1$ K, corresponding to thermal inertias $>400\ \mathrm{J\,m^{-2}\,s^{-1/2}\,K^{-1}}$ (refs 11, 12) and unconsolidated particle diameters $>\sim 1$ mm (ref. 13), indicating that all of the floor materials are coarse-grained. The low TES albedo (<0.12; ref. 7) and low spectrally derived dust cover index[14] confirm that these are dust-free surfaces.

Compositional mapping with THEMIS multi-spectral and TES hyperspectral[15] IR imaging shows distinct variations across the caldera floor and the surrounding flanks of the volcano (Figs 3 and 4). The two primary floor units are a 'magenta' unit (unit A) that occurs in an area ~12 by 12 km on the central portion of the caldera floor with several nearby outliers, and a 'blue' unit (unit B) that covers much of the eastern and western portions of the caldera floor (Fig. 4). Several 5–20-km-sized flow units that are spectrally similar to unit A occur 50–60 km to the south along an arcuate trend (Fig. 3).

Unit A is lobate with steep margins, stands ~80 m above the floor,

[1]Department of Geological Sciences, Arizona State University Tempe, Arizona 85287, USA. [2]Department of Earth and Planetary Sciences, University of Tennessee, Knoxville, Tennessee 37996, USA. [3]Institute of Geophysics and Planetology, University of Hawaii, Honolulu, Hawaii 96822, USA. [4]University of Colorado, Boulder, Colorado, USA. [5]US Geological Survey, Emeritus, Carson City, Nevada 89703, USA. [6]Malin Space Science Systems, San Diego, California 92191, USA.

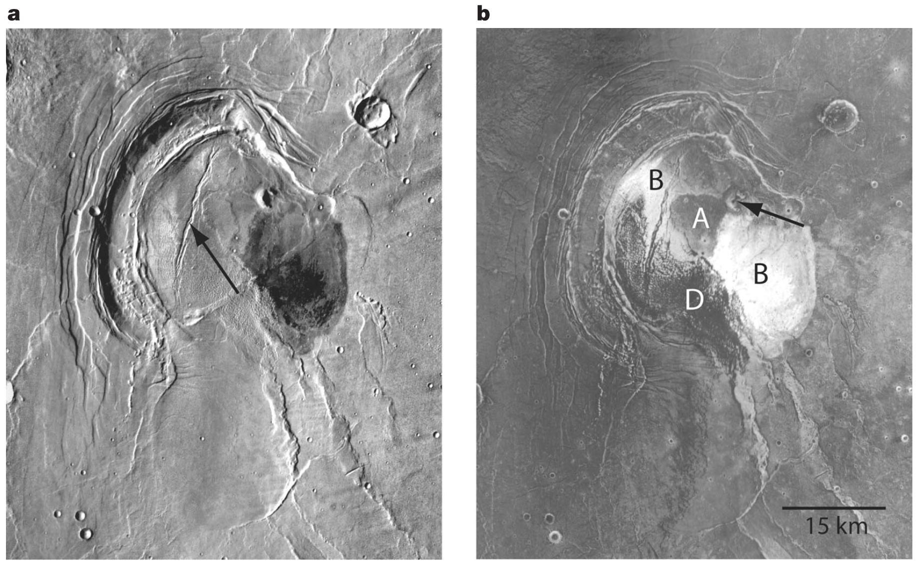

Figure 1 | **Daytime and night-time mosaics of THEMIS thermal images of the summit region of Syrtis Major showing the Nili Patera caldera and surrounding lava plains.** **a**, Daytime mosaic. The caldera is delineated on the western side by concentric ring fractures. The cool (dark) region of the southeast caldera floor is the bedrock surface. A N–S-trending graben system (arrow) was produced by doming after floor emplacement. **b**, Night-time mosaic. The bedrock surfaces of unit B are bright (warm) at night with temperatures >210 K. The colder (dark) lobate unit A (A) is clearly delineated from the surrounding caldera floor by its uniformly lower temperatures and is associated with a construct (arrow). Dunes (D) cover much of the southeastern portions of the caldera floor. Each mosaic is centred near 9° N, 67° E. North is towards the top in all figures.

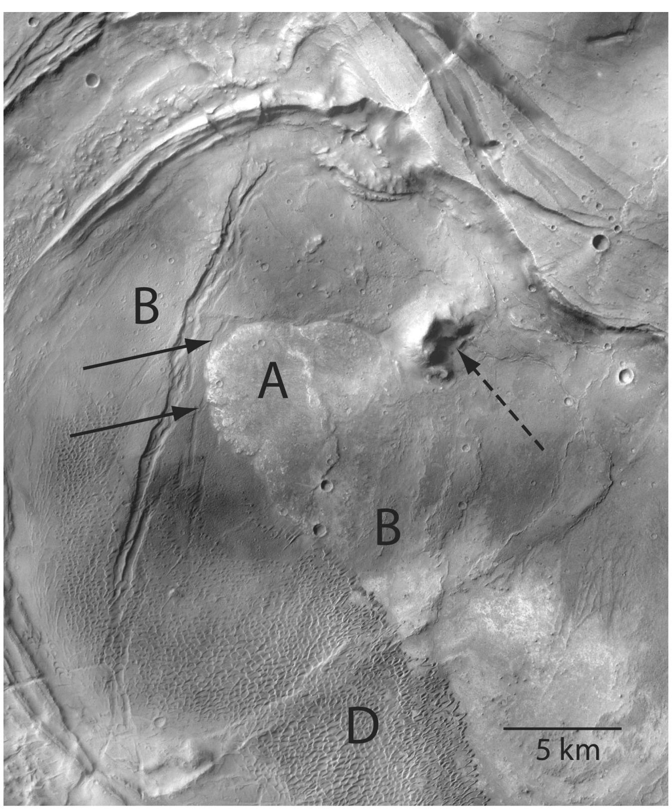

Figure 2 | **The floor of the Nili Patera caldera seen in a mosaic of THEMIS visual images.** Unit A is an ~80-m-thick lobate flow feature that is stratigraphically above older floor units, as evidenced by the superposition relationship of unit A on sections of the underlying N–S trending graben system (arrows) that cut unit B. Flow unit A appears to originate from a 300-m-high construct (dashed arrow) also identified in Fig. 1. Barchan dunes (D) cover the southern and southwestern caldera floor.

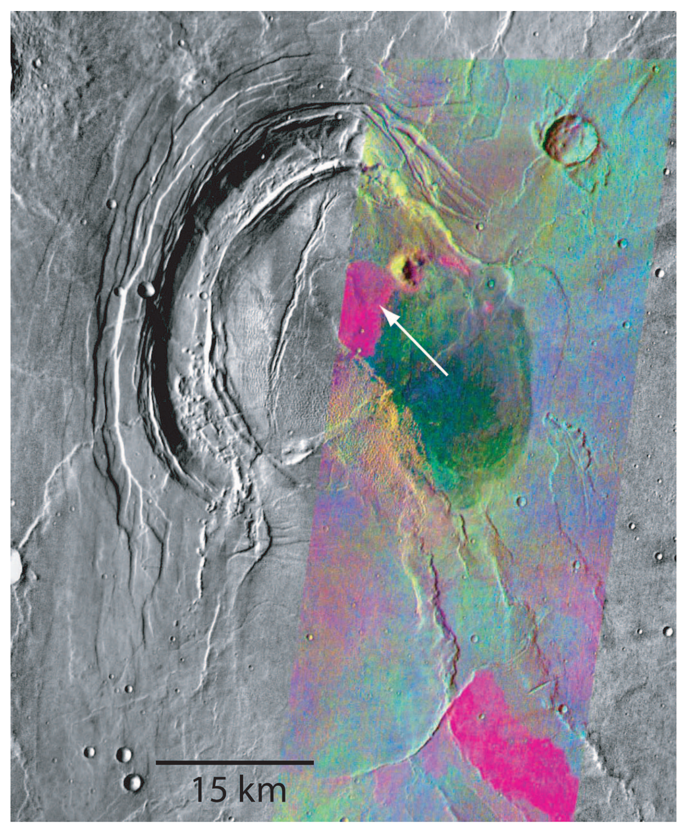

Figure 3 | **Compositional unit map of Nili Patera and the surrounding lava plains derived from a THEMIS multispectral IR image.** THEMIS bands 9, 7 and 5 were processed using a decorrelation stretch to enhance the spectral differences[49], and are shown superimposed of the daytime IR mosaic for geologic context. Unit A is bright magenta and occurs in a lobate flow unit on the caldera floor and several small outliers to the west. Flows spectrally similar to unit A also occur outside the caldera in units that appear to emanate from a positive-relief linear feature. These flows also differ significantly in composition from their surroundings.

and has a surface morphology that is distinct from the surrounding floor materials (Fig. 2). It surrounds a relatively steep-sided (~10°), ~300-m-high cone, and post-dates the unit-B floor materials based on its superposition across one of the grabens formed in unit B (Fig. 2). Units A and B have similarly relatively high crater densities, indicating similarly old ages. Night-time temperatures are uniform within units A and B, but differ significantly between them, with unit B consistently 8–9 K warmer than unit A (Fig. 1b), indicating a significant difference in the average particle size or rock abundance between these units[5,11].

The mineral compositions and abundances of units A and B were determined using a linear least-squares deconvolution[16,17] that has been applied extensively to the analysis of TES, Miniature TES (Mini-TES)[18,19] and laboratory spectra[1,7,8,20–23]. Unit B is composed of 35% plagioclase, 25% high-Ca clinopyroxene, 10% orthopyroxene, 10% sulphate, and minor glass, olivine, and carbonate components (Fig. 5a). Unit A is 30% plagioclase, 30% high-Si glass, and 15% clinopyroxene, with lesser sulphate and minor orthopyroxene and carbonate components (Fig. 5b).

Unit B is a basalt that is similar in composition to the typical basalt (surface type I) mapped using orbital TES data throughout much of the ancient cratered terrain[1,2]. Basalts of similar composition have been identified at the Opportunity landing site in the Meridiani plain[19,24].

The composition of unit A is much more silicic than the adjacent basalt, with high-Si glass, plagioclase and clinopyroxene. The spectral bands near 1,075 and 475 cm^{-1} are well matched by a SiO_2-K_2O glass (Fig. 5b). Illite clay and some zeolites, which can develop from the aqueous alteration of high-Si glass, provide spectral alternatives to silica glass, although neither matches unit A as well as glass (Fig. 6), so we conclude that glass is a major component in unit A.

The derived SiO_2 abundance[21,25,26] of unit A is 60–63 wt%, as compared to values of 56 to 59 wt% for TES surface type II[26]. Given the probable contribution of the surrounding basaltic terrain to the deconvolved TES spectra, this derived SiO_2 abundance is a lower limit. Unit A thus has the highest silica abundance, and the most-evolved rock composition, of any volcanic unit yet found on Mars, with a composition corresponding to the low-silica end of the dacite composition field. A high-viscosity glassy dacite composition is consistent with unit A's occurrence as a relatively short, thick flow, its association with a steep-sided volcanic cone, and its distinct morphology.

The sulphate abundance derived for both units is slightly higher than the background abundance found for much of Mars[7]. The short-wavelength edge of the IR absorption at ~1,200 cm^{-1} is shifted to shorter wavelengths than typical for either type-I or -II material. This shift is characteristic of the Ca and Mg sulphates observed by Mini-TES at Meridiani Planum[19], and suggests that sulphates may

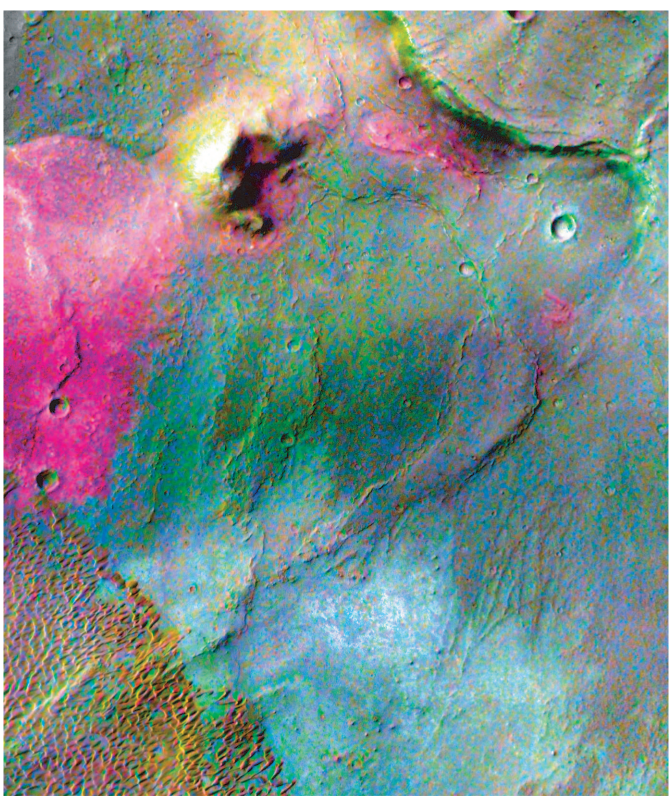

Figure 4 | The compositional units of the Nili Patera floor. A portion of the multispectral THEMIS IR image (Fig. 3) is superimposed on an 18 m per pixel THEMIS visual image. The colours are derived from the decorrelation stretch of IR bands 9, 7 and 5. This superposition illustrates the correlation between the composition and morphologic properties of the Nili Patera floor materials. The lobate flow (magenta; unit A) and associated cone are have a unique composition from the lavas that comprise most of the caldera floor (unit B; blue). Small outliers of unit-A material are visible east of the cone. Image width is 16 km.

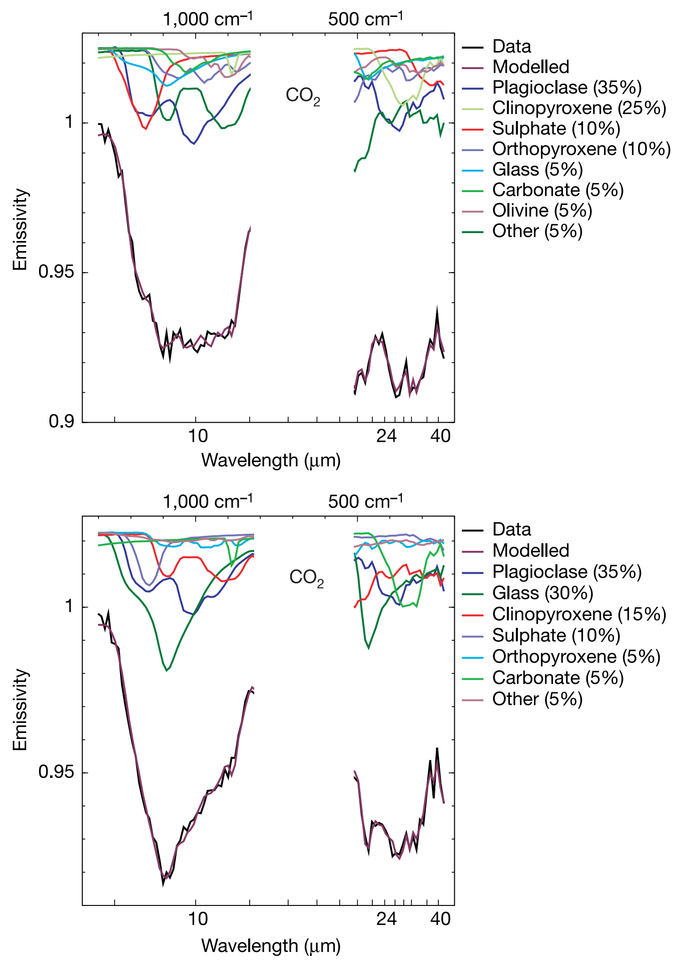

Figure 5 | Mineral composition and abundance of Nili Patera floor units derived from deconvolution of TES spectra. a, Unit B has the mineral composition and abundance of basalt. Mineral abundances derived from the deconvolution model have been rounded to the nearest 5%. Minor components with <2.5% abundance have been grouped into the category 'Other'. The endmember spectra have been scaled on the basis of their derived abundance to indicate their relative contribution to the measured spectrum. Wavelengths from ~12 to 19 μm are blocked by absorption of atmospheric CO_2. **b**, The mineralogy of unit A, including a high abundance of Si-K glass (30%) and plagioclase (30%), indicates that this flow unit is dacite in composition.

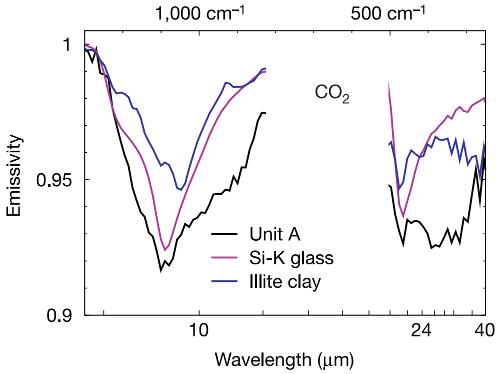

Figure 6 | Comparison of the spectra of Si-K glass and illite clay with the spectrum of unit A. Glass provides a better match than either clay or zeolites to the spectral bands from ~900 to 1,050 cm^{-1} and 460 to 500 cm^{-1}.

be present within this region, possibly associated with volcanic emanations or fumaroles.

THEMIS eight-point spectra closely match the TES spectra and were deconvolved to provide a quantitative measure of the dacite abundance at 100-m scales (Fig. 7). Unit A is a coherent dacite unit that includes the cone, suggesting that the flow originated from the same source vent as the cone. The spectrally distinct flows to the south are also dacites that were probably erupted from a separate source (Fig. 7). Both the THEMIS and TES spectra suggest that the dunes are composed primarily of basalt, probably eroded from the upwind bedrock exposure. Along their western margin the dunes show subtle colour and spectral variations that suggest an influx of dacitic sands.

We interpret unit B to be basaltic lavas that covered the floor of the caldera following its collapse. Unit A is a later, high-silica, glassy volcanic unit associated with, and probably emanating from, a volcanic cone. Fractional crystallization of magma within a chamber commonly results in variations in the silica content of the erupted lavas over time. It appears that magmatic evolution has occurred within Syrtis Major, producing low-silica basalts followed by higher-silica glassy dacites in cones and flows. Orbital TES data have identified two surface components (TES surface type I and II; ref. 2) whose fundamental difference is silica content. The high-silica component in type-II material, which extends across much of the northern plains and throughout the southern highlands, has been attributed to primary volcanic glass in a basaltic andesite[2]. Alternative interpretations include high-silica, poorly crystalline materials or other weathering/alteration products[27–31], in part based on the apparent necessity for a wet mantle to produce large volumes of andesitic material[26]. The close proximity and similar geologic ages of units A and B argue against compositional differences based on differential weathering, whereas the geologic relationships support differences in primary volcanic composition. We therefore conclude that, at least locally, high-silica lavas have been produced on Mars, and could be an important component of the globally occurring TES type-II material.

Olivine-rich basalt

The occurrence of olivine is important because: (1) it indicates silica undersaturation (a critical parameter in recognizing primitive, mantle-derived magmas); and (2) it is readily weathered under common aqueous conditions and thus provides an indicator of environmental conditions in the time following rock emplacement.

Olivine-rich rocks have been identified from orbit at regional scales in several locations[23,32]. THEMIS data show that these occurrences are common at localized (hundreds of metres) scales[5,33–35]. An example of an olivine-rich unit occurs on the floor of a 60-km-diameter crater in Aurorae Planum immediately south of western Ganges Chasma[33,36] (Fig. 8). This unit is mapped as a distinct spectral unit using THEMIS, and positively identified as olivine-rich basalt using TES spectra. It is 10–12 K warmer than the surrounding terrain in night-time THEMIS images, with a thermal inertia $>800\,J\,m^{-2}\,s^{-1/2}\,K^{-1}$, indicating the presence of significant rocky material. This unit has been incised 15 to 20 m by channels (Fig. 8), providing additional evidence that it is a competent layer. The olivine basalt forms the uppermost layer in a crater that is superimposed on the top of the thick sequence of layered rocks that comprise Aurorae Planum. Its position, composition, and morphology suggest that it was emplaced as a lava flow at a late stage in plains formation.

A similar olivine basalt layer is exposed 4.5 km below the surface, 600 km to the east, in the walls of Ganges Chasma. This ~100-m-thick unit crops out over an area 30 by 100 km in size[5]. The composition of this layer is basalt with >~15% olivine with an Mg/(Mg + Fe) ratio of 0.60 to 0.70 (Fo60-70)[5]; the unit exposed below it on the floor of Ganges Chasma is determined from TES data to be basaltic.

The similarity in the derived composition of the Ganges and Aurorae Planum units suggests that they formed by similar processes, most probably eruption as lava flows. The occurrence of the Ganges unit at a significantly lower stratigraphic level than the Aurorae Planum unit suggests that olivine-rich basalts were erupted episodically at significantly different times throughout the formation of the martian plains.

Picritic basalts have also been observed *in situ* by the Spirit rover in the Gusev crater using IR, Mossbauer, and alpha particle X-ray spectra[18,37–39]. Similar examples of olivine-rich basalts have been identified using both TES data and THEMIS data in Ares Valles[35], Nili Fossae[34], and elsewhere[33,36]. This growing inventory of olivine basalts suggests that mafic basalts may be a relatively common variant of martian basalts. They probably represent less-evolved lavas or contain higher abundances of cumulates or mantle xenoliths than typical basalts.

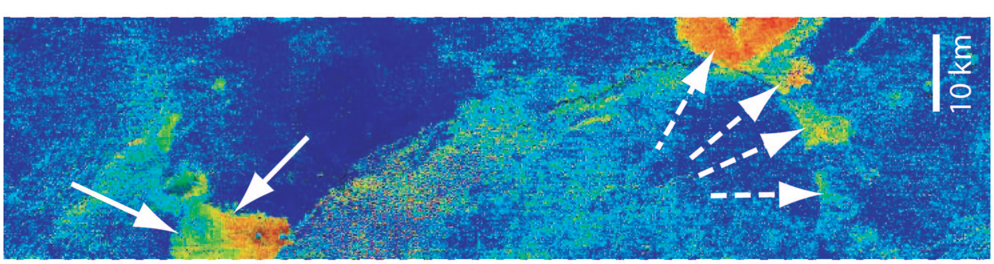

Figure 7 | Dacite abundance derived from the deconvolution of a THEMIS eight-band multi-spectra IR image of Nili Patera. Red colour represents 80% dacite abundance; blue is 0% abundance. Green and yellow colours also represent high (>50%) dacite abundance, but with the shallower spectral contrast that is probably due to smaller particle size. In addition to the flow and cone mapped as unit A (arrows), several large dacite flows occur to the south (dashed arrows). North is towards '9 o'clock'.

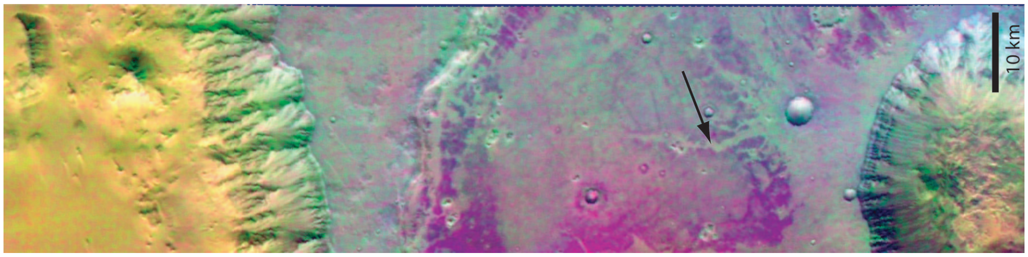

Figure 8 | THEMIS compositional map of a portion of a crater in Aurora Planum. The purple regions are outcrops of olivine-rich basalt. This basalt unit has been incised by channels (arrow), indicating that it is a competent rock layer. THEMIS image I01513001 centred near 308° E; 8° S. Image width is 32 km; north is towards '9 o'clock'.

Quartz-bearing granitoid rocks

Quartz has not been recognized on Mars at regional or global scales. Its presence is important for recognizing igneous rocks that have experienced extreme fractionation. Unlike olivine, quartz persists during sedimentary weathering and transport and, if ever formed, should persist in primary or sedimentary rock units.

THEMIS observations have revealed the presence of quartz-bearing rocks exposed in crater central uplifts in two 30-km-diameter craters on the northern flank of the Syrtis Major volcanic construct[40] (Fig. 9). The corresponding TES spectra match laboratory spectra of granitoid rocks composed primarily of quartz and plagioclase[40]. The association of these outcrops with central peaks suggests that these rocks were uplifted from depths of several kilometres by the impact process[40]. The two craters in which these rocks are found are 95 km apart, but no rocks of similar composition have been found on the planet, suggesting that they are part of an unusual regional rock unit that is postulated to be a single granitoid pluton[40].

All of the remote, *in situ*, and martian meteorite analyses to date indicate that Mars is dominated by ultramafic to possibly intermediate volcanic compositions[1,2,4,7,18,19,32,37,41,42]. While fractional crystallization of magmas can produce highly differentiated, high-silica melts[43], the volumes required to produce the Syrtis Major pluton would produce enormous quantities of mafic cumulates[40], which are not observed in any central peaks. A more likely process is partial melting of thick sequences of pre-existing basaltic rocks at relatively low pressures to form high-silica trondhjemites and tonalites[40,43,44].

Implications for crustal formation and evolution

Multi-spectral IR imaging at 100-m scales has produced petrologic maps that are, for the first time, at scales appropriate for studying local geologic processes. At these scales we have identified rock units in basaltic terrains that have olivine abundances of >20%, which on Earth would be classified as picrites. These rocks have been identified in eroded canyon walls and crater floors of ancient terrains in several areas, suggesting that they may be relatively common throughout the ancient martian crust but remain unexposed in most locations. Local eruptive sequences are observed in the Syrtis Major volcano that appear to have evolved in composition from basaltic to dacitic, demonstrating that fractional crystallization occurs in martian magma chambers. This diversity in composition is the result of igneous processes analogous to those found in large volcanic complexes on Earth. Rare occurrences of exposed quartz-bearing granitoid rocks have been discovered on Mars, suggesting the formation of highly evolved magmas. Taken together, these observations show that the martian crust, while dominated by basalt, has produced a diversity of igneous materials whose range in composition from ultramafic to highly silicic rivals that found on the Earth.

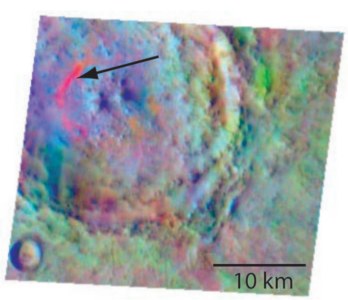

Figure 9 | The occurrence of quartz-bearing granitoid rocks mapped using THEMIS multi-spectral IR imaging. This compositional unit map of a 30-km-diameter unnamed crater in Syrtis Major shows the occurrence of quartz-bearing granitoid rocks (red colour; arrow) within the central peak[40]. THEMIS bands 6, 5 and 4 were processed using a decorrelation stretch to enhance the spectral differences[49].

METHODS

The spectral deconvolution of TES spectra was done using averages of 5–10 atmospherically corrected TES spectra that were isolated from each unit[1,8,45,46]. The TES has collected over 200 million IR spectra of the martian surface with 3×8 km spatial resolution[7]. These spectra have been used extensively to map global and regional lithologic units[1,2,7,8,30,32,36,40,47]. Each spectrum collected from units A and B was analysed using the same 36-component endmember library used for TES global mapping[8]. This library was constructed from laboratory minerals and TES surface dust spectra[48], and contained representative suites of pyroxene, feldspar, olivine, sulphate, carbonate, and oxide minerals. Spectral effects due to small particle sizes ($<\sim 60\,\mu m$; ref. 17) can be ignored owing to the coarse-grained materials that are shown to comprise both units A and B, based on the night-time temperature and derived thermal inertia. Uncertainties for the mineral abundances derived from the deconvolution are estimated to be $\pm 5\%$, based on laboratory analyses and *in situ* validation of spectra acquired by the Mini-TES on the MER rovers[1,8,18–20]. Recent *in situ* measurements from the Mössbauer[38], Mini-TES[18], and Alpha Particle X-ray spectrometers[39] on the Mars Exploration Rovers have determined mineral compositions that have verified the TES determinations from orbit[18,37], providing higher confidence in interpretations made elsewhere on the planet.

Deconvolution of the THEMIS spectra was done in a similar manner to the TES analysis, but used the atmospherically corrected TES spectra of units A (dacite) and B (basalt). These spectra were convolved to the THEMIS spectral bandpasses, and used as endmembers in the deconvolution of the THEMIS multi-spectral IR image. This method provides a quantitative measure of abundance of dacite and basalt. The dacite abundance derived using this method is shown in Fig. 7.

Received 13 November 2004; accepted 7 April 2005.
Published online 6 July 2005.

1. Christensen, P. R., Bandfield, J. L., Smith, M. D., Hamilton, V. E. & Clark, R. N. Identification of a basaltic component on the Martian surface from Thermal Emission Spectrometer data. *J. Geophys. Res.* **105,** 9609–9622 (2000).
2. Bandfield, J. L., Hamilton, V. E. & Christensen, P. R. A global view of Martian volcanic compositions. *Science* **287,** 1626–1630 (2000).
3. Soderblom, L. A. in *Mars* (eds Kieffer, H. H., Jakosky, B. M., Snyder, C. W. & Matthews, M. S.) 557–593 (Univ. Arizona Press, Tucson, 1992).
4. Mustard, J. F. & Sunshine, J. M. Seeing through the dust: Martian crustal heterogeneity and links to the SNC meteorites. *Science* **267,** 1623–1626 (1995).
5. Christensen, P. R. *et al.* Morphology and composition of the surface of Mars: Mars Odyssey THEMIS results. *Science* **300,** 2056–2061 (2003).

6. Christensen, P. R. *et al.* Detection of crystalline hematite mineralization on Mars by the Thermal Emission Spectrometer: Evidence for near-surface water. *J. Geophys. Res.* **105,** 9623–9642 (2000).
7. Christensen, P. R. *et al.* The Mars Global Surveyor Thermal Emission Spectrometer experiment: Investigation description and surface science results. *J. Geophys. Res.* **106,** 23823–23871 (2001).
8. Bandfield, J. L. Global mineral distributions on Mars. *J. Geophys. Res.* **107,** doi:10.1029/2001JE001510 (2002).
9. Schaber, G. G. Syrtis Major: A low-relief volcanic shield. *J. Geophys. Res.* **87,** 9852–9866 (1982).
10. Smith, D. E. *et al.* Mars Orbiter Laser Altimeter: Experiment summary after the first year of global mapping of Mars. *J. Geophys. Res.* **106,** 23689–23722 (2001).
11. Kieffer, H. H. *et al.* Thermal and albedo mapping of Mars during the Viking primary mission. *J. Geophys. Res.* **82,** 4249–4292 (1977).
12. Mellon, M. T., Jakosky, B. M., Kieffer, H. H. & Christensen, P. R. High resolution thermal inertia mapping from the Mars Global Surveyor Thermal Emission Spectrometer. *Icarus* **148,** 437–455 (2000).
13. Presley, M. A. & Christensen, P. R. Thermal conductivity measurements of particulate materials, Part II: Results. *J. Geophys. Res.* **102,** 6551–6566 (1997).
14. Ruff, S. W. & Christensen, P. R. Bright and dark regions on Mars: Particle size and mineralogical characteristics based on Thermal Emission Spectrometer data. *J. Geophys. Res.* **107,** doi:10.1029/2001JE001580 (2002).
15. Ruff, S. W. & Hamilton, V. E. Mineralogical anomalies in Mars Nili Patera caldera observed with Thermal Emission Spectrometer data. *Lunar Planet. Sc.* **XXXII,** abstr. 2186 [CD-ROM] (2001).
16. Adams, J. B., Smith, M. O. & Johnson, P. E. Spectral mixture modeling: A new analysis of rock and soil types at the Viking Lander 1 site. *J. Geophys. Res.* **91,** 8098–8112 (1986).
17. Ramsey, M. S. & Christensen, P. R. Mineral abundance determination: Quantitative deconvolution of thermal emission spectra. *J. Geophys. Res.* **103,** 577–596 (1998).
18. Christensen, P. R. *et al.* Initial results from the Miniature Thermal Emission Spectrometer experiment at the Spirit landing site at Gusev crater. *Science* **305,** 837–842 (2004).
19. Christensen, P. R. *et al.* Mineralogy at Meridiani Planum from the Mini-TES experiment on the Opportunity rover. *Science* **306,** 1733–1739 (2004).
20. Feely, K. C. & Christensen, P. R. Quantitative compositional analysis using thermal emission spectroscopy: Application to igneous and metamorphic rocks. *J. Geophys. Res.* **104,** 24195–24210 (1999).
21. Wyatt, M. B., Hamilton, V. E., McSween, H. Y. Jr, Christensen, P. R. & Taylor, L. A. Analysis of terrestrial and martian volcanic compositions using thermal emission spectroscopy: I. Determination of mineralogy, chemistry, and classification strategies. *J. Geophys. Res.* **106,** 14711–14732 (2001).
22. Hamilton, V. E., Wyatt, M. B., McSween, H. Y. Jr & Christensen, P. R. Analysis of terrestrial and martian volcanic compositions using thermal emission spectroscopy: II. Application to martian surface spectra from MGS TES *J. Geophys. Res.* **106,** 14733–14747 (2001).
23. Hamilton, V. E., Christensen, P. R., McSween, H. Y. Jr & Bandfield, J. L. Searching for the source regions of martian meteorites using MGS TES: Integrating martian meteorites into the global distribution of igneous materials on Mars. *Meteorit. Planet. Sci.* **38,** 871–885 (2003).
24. Rieder, R. *et al.* Chemistry of rocks and soils at Meridiani Planum from the Alpha Particle X-ray Spectrometer. *Science* **306,** 1746–1749 (2004).
25. Hamilton, V. E. & Christensen, P. R. Determining the modal mineralogy of mafic and ultramafic igneous rocks using thermal emission spectroscopy. *J. Geophys. Res.* **105,** 9717–9734 (2000).
26. McSween, H. Y. Jr, Grove, T. L. & Wyatt, W. B. Constraints on the composition and petrogenesis of the martian crust. *J. Geophys. Res.* **108,** doi:10.1029/2003JE002175 (2003).
27. Wyatt, M. B. & McSween, H. Y. Jr Spectral evidence for weathered basalt as an alternative to andesite in the northern lowlands of Mars. *Nature* **417,** 263–266 (2002).
28. Wyatt, M. B., McSween, H. Y. Jr, Tanaka, K. L. & Head, J. W. III Global geologic context for rock types and surface alteration on Mars. *Geology* **32,** 645–648 (2004).
29. Kraft, M. D., Michalski, J. R. & Sharp, T. G. High-silica rock coatings: TES surface-type 2 and weathering in Mars. *Lunar Planet. Sci.* **XXXV,** abstr. 1936 [CD-ROM] (2004).
30. Ruff, S. W. Spectral evidence for zeolite in the dust on Mars. *Icarus* **168,** 131–143 (2004).
31. Michalski, J. R., Kraft, M. D., Sharp, T. G., Williams, L. B. & Christensen, P. R. Mineralogical constraints on the high-silica Martian surface component observed by TES: Clay-rich mineralogy does not sufficiently explain the Acidalia Planitia-type spectra. *Icarus* (in the press).
32. Hoefen, T. *et al.* Discovery of olivine in the Nili Fossae region of Mars. *Science* **302,** 627–630 (2003).
33. Hamilton, V. E. & Christensen, P. R. Detailed mineralogical analyses of Martian meteorite-like terrains using MGS TES and Odyssey THEMIS data. *Lunar Planet. Sci.* **XXXIV,** abstr. 1982 [CD-ROM] (2003).
34. Hamilton, V. E. & Christensen, P. R. Evidence for extensive olivine-rich bedrock on Mars. *Geology* (in the press).
35. Rogers, A. D., Christensen, P. R. & Bandfield, J. L. Compositional heterogeneity of the ancient martian crust: Analysis of Ares Vallis bedrock the THEMIS and TES data. *J. Geophys. Res.* (submitted).
36. Hamilton, V. E., Christensen, P. R. & McSween, H. Y. Jr Global constraints on the source regions of martian meteorites from MGS TES data. *Meteorit. Planet. Sci.* **37,** 59 (2003).
37. McSween, H. Y. Jr *et al.* Basaltic rocks analyzed by the Spirit rover in Gusev crater. *Science* **305,** 842–845 (2004).
38. Morris, R. V. *et al.* Mineralogy at Gusev crater from the Mössbauer spectrometer on the Spirit rover. *Science* **305,** 833–836 (2004).
39. Gellert, R. *et al.* Chemistry of rocks and soils at Gusev crater from the Alpha Particle X-ray Spectrometer. *Science* **305,** 829–832 (2004).
40. Bandfield, J. L., Hamilton, V. E., Christensen, P. R. & McSween, H. Y. Jr Identification of quartzofeldspathic materials on Mars. *J. Geophys. Res.* **109,** doi:10.1029/2004JE002290 (2004).
41. McSween, H. Y. Jr What have we learned about Mars from SNC meteorites. *Meteoritics* **29,** 757–779 (1994).
42. McSween, H. Y. Jr The rocks of Mars, from far and near. *Meteorit. Planet. Sci.* **37,** 7–25 (2002).
43. Clark, D. B. *Granitoid Rocks* (Chapman and Hall, New York, 1992).
44. Barker, F. in *Trondhjemites, Dacites, and Related Rocks* (ed. Barker, F.) 1–12 (Elsevier, New York, 1979).
45. Smith, M. D., Bandfield, J. L. & Christensen, P. R. Separation of atmospheric and surface spectral features in Mars Global Surveyor Thermal Emission Spectrometer (TES) spectra: Models and atmospheric properties. *J. Geophys. Res.* **105,** 9589–9608 (2000).
46. Bandfield, J. L. & Smith, M. D. Multiple emission angle surface-atmosphere separations of Thermal Emission Spectrometer data. *Icarus* **161,** 47–65 (2003).
47. Christensen, P. R., Morris, R. V., Lane, M. D., Bandfield, J. L. & Malin, M. C. Global mapping of Martian hematite mineral deposits: Remnants of water-driven processes on early Mars. *J. Geophys. Res.* **106,** 23873–23885 (2001).
48. Christensen, P. R. *et al.* A thermal emission spectral library of rock forming minerals. *J. Geophys. Res.* **105,** 9735–9738 (2000).
49. Gillespie, A. R. Spectral mixture analysis of multispectral thermal infrared images. *Remote Sens. Environ.* **42,** 137–145 (1992).

Acknowledgements We thank the Odyssey Spacecraft Teams at Lockheed Martin and the Jet Propulsion Laboratory, the THEMIS Operations Team at ASU, led by G. Mehall, the ASU Software Development Team, led by N. Gorelick, and the USGS ISIS Software Development Team, led by J. Torson.

Author Information Reprints and permissions information is available at npg.nature.com/reprintsandpermissions. The authors declare no competing financial interests. Correspondence and requests for materials should be addressed to P.C. (phil.christensen@asu.edu).